The International Journal of Advanced Manufacturing Technology
https://doi.org/10.1007/s00170-026-19274-0

ORIGINAL ARTICLE

Integrated assessment of mechanical properties and environmental footprint in MSLA 3D printing

Chiara Mignanelli[1] · **Michela Simoncini**[1] · **Tommaso Verdini**[1]

Received: 30 March 2026 / Accepted: 29 September 2026
© The Author(s) 2026

Abstract
Masked Stereolithography is an additive manufacturing technology widely adopted for industrial and biomedical applications due to its high accuracy and surface quality. Nevertheless, the combined effects of process parameters on mechanical performance and environmental sustainability remain insufficiently explored. This study presents an integrated assessment of the mechanical properties and environmental impacts of printed components, aiming to identify optimal printing conditions. Specimens were produced using a commercial photocurable resin by varying exposure time (4–12 s), layer thickness (0.01–0.09 mm), and LED light intensity (50–100%), following a Box–Behnken Design of Experiments with 15 printing conditions. Tensile and flexural properties were evaluated according to ASTM D638 and ASTM D790 standards, while energy consumption during printing and post-processing was experimentally measured. Non-linear multiple regression models were developed to predict mechanical properties and energy consumption, and a cradle-to-gate Life Cycle Assessment was performed in compliance with ISO 14040–44 standards using Global Warming Potential as the impact category. Results indicate that longer exposure times and higher LED intensities improve tensile and flexural strength and stiffness by enhancing polymer cross-linking, although diminishing returns occur at higher levels. Reduced layer thickness increases mechanical performance but leads to higher energy consumption and environmental impacts due to extended printing times. The regression models showed high predictive accuracy ($R^2 > 96\%$, MAPE $< 8\%$). Life Cycle Assessment results reveal that the material phase contributes up to 90% of total environmental impacts, while intermediate layer thicknesses (~0.05 mm) provide the best trade-off between mechanical performance and sustainability. This work provides practical guidelines for optimizing Masked Stereolithography process parameters toward sustainable additive manufacturing.

Keywords Masked SLA · Mechanical testing · Multiple Non-linear Regression · Environmental sustainability

1 Introduction

Additive Manufacturing (AM) technologies are gaining an increasing interest in many industrial fields for both prototyping and the realization of commercial components [1]. AM offers many advantages in terms of impacts reduction by allowing the production of lightweight and high-quality parts with complex geometries. [2–4]

Among the additive manufacturing technologies, stereolithography (SLA), based on the photopolymerization of a liquid photocurable resin under the action of an ultraviolet (UV) light source, is one of the most well-established and used in industrial applications [1, 5–7].

Specifically, the Masked Stereolithography (MSLA) is one of the most advanced variants of the SLA and it gained many interests since it guarantees high precision, low cost and greater speed as compared to similar processes, such as the conventional SLA and Digital Light Processing (DLP) [8, 9].

The MSLA technique requires a Liquid–Crystal Display (LCD) module which works as a digital mask to project the

✉ Tommaso Verdini
t.verdini@pm.univpm.it

Chiara Mignanelli
c.mignanelli@pm.univpm.it

Michela Simoncini
m.simoncini@univpm.it

[1] Department of Industrial Engineering and Mathematical Sciences, Università Politecnica Delle Marche, Via Brecce Bianche 12, Ancona 60131, Italy

Published online: 09 October 2026

image of the entire model layer directly onto the photopolymer resin surface. This method is different from the conventional SLA, in which each section of the layer is traced point by point by using a laser source, and from DLP technology, in which the whole layer image is projected by means of a Digital Micromirror Device (DMD).

Since the process requires solidifying only desired areas of each layer, an LCD panel is used to selectively block or allow the passage of light in the form of UV radiation emitted by the LED light source [10]. This system ensures a uniform light distribution across the whole build area, involving an improvement of the production speed and a reduction of mechanical wear with respect to laser-based scanning technologies. To obtain the whole part, each layer is formed by solidifying the liquid resin and repeating the process layer by layer until the part is fully built.

Due to its high dimensional accuracy and smooth surface finish, MSLA technology is particularly suitable for industrial and biomedical applications [1, 10].

The quality of the layer's solidification and, consequently, the mechanical and structural properties of the final part depend on the process parameters, such as the exposure time, layer thickness and UV light intensity [11–13]. Therefore, the evaluation of the effect of the printing parameters on the material mechanical properties is crucial to ensure structural strength and repeatability of the manufactured components. Valizadeh et al. demonstrated that a significant printing parameter is the UV exposure time since it directly affects the degree of polymer cross-linking and, consequently, the mechanical properties such as elastic modulus, tensile strength, and deformation capacity [14]. Recent studies showed that longer exposure times enhance strength and stiffness but may reduce elongation to failure, highlighting the need for a compromise in parameter optimization [10, 15, 16]. Moreover, variations of the UV light intensity can influence the depth and the uniformity of solidification, affecting the material's microstructure and mechanical properties. Another parameter affecting the material properties is layer thickness, as printing thin layers typically results in improved print resolution and surface quality, although production time significantly increases [17].

Recent research on stereolithography (SLA) 3D printing has shown increasing interest in optimizing process parameters to enhance mechanical, dimensional, and surface quality outcomes. Several studies have investigated a variety of influencing parameters through both experimental and computational approaches. For instance, Vidal et al. developed a mathematical model integrating parameters, such as build orientation, lifting speed, lifting distance, and exposure time, to optimize mechanical properties including hardness, surface roughness, and strength of SLA printed parts [18]. Chockalingam et al. applied a Design of Experiments (DoE) methodology using a Box-Behnken Design (BBD) to analyze the effect of layer thickness, part orientation, and post-curing time on the strength of SLA fabricated components [19]. The influence of build orientation was specifically addressed in another study, in which the mechanical performance of ASTM D-638 Type I specimens was evaluated, showing a direct correlation between build orientation and tensile strength [20]. As far as the material modelling is concerned, Quintana et al. implemented an elastoplastic constitutive model to accurately describe the mechanical response of SLA-printed materials as a function of layer thickness and build orientation [20]. Temiz analyzed the influence of the exposure time, layer thickness, and sample orientation on the tensile properties and printing time by using a Response Surface Methodology (RSM) framework, providing insight into trade-offs between process time and properties [12]. In this framework, Borra and Neigapula studied the dimensional accuracy of the SLA printed component as a function of exposure time, layer thickness, and build orientation using the Taguchi method, demonstrating the significant effect of these process parameters on achieving tight tolerances [11]. In the dental field, Mhmood and AL-Karkhi utilized a combined Taguchi and RSM approach to optimize surface roughness and dimensional features, focusing the attention on process parameters such as bottom exposure time, number of bottom layers, and exposure time [21]. Furthermore, the response surface methodology was applied by Weheba and Sanchez-Marsa to correlate the flatness and surface roughness of SLA printed components to process parameters such as fill cure depth, hatch overcure, and Z-level wait [22]. Also, Singh et al. concentrated on predicting and optimizing surface roughness by analyzing layer height, exposure time, light-off delay, and build orientation, emphasizing the correlation between fine feature resolution and print settings [23]. The assessment of dimensional accuracy and geometry resolution was also addressed by Cotabarren et al. in [24], in which a model based on the printing angle in X and Y axes, as well as position on the build tray and layer thickness, was introduced highlighting the spatial dependency of print precision.

Despite the wide use of MSLA in advanced applications, scientific literature lacks an overall evaluation of the mechanical properties related to combined process parameters and environmental sustainability.

In this context, the present study aims to investigate the combined effect of printing parameters, such as the exposure time, layer thickness, and led intensity, on both tensile and flexural properties of MSLA printed specimens. In addition, the energy consumption of the printing process was recorded and used to evaluate the environmental impacts of stereolithography process and printed parts by means of the Life Cycle Assessment (LCA) analysis. The relationship

between the mechanical properties of SLA printed specimens and the ecological footprint was evaluated as a function of the different process parameters, to identify the optimal process parameters combination.

The results of this research are extremely useful and interesting for users and suppliers of SLA equipment because they highlight how process parameters can be chosen to simultaneously optimize the mechanical properties of printed components and reduce the environmental impact of the process. In this way, the manuscript aims to provide practical guidelines on MSLA technology, expanding the potential application of the process in industrial fields in which a combination of high mechanical performances and reduced environmental loads are required.

2 Materials and methods

2.1 Material and masked stereolithography process

The material investigated is an ELEGOO standard commercial translucent LCD photocurable resin. It is composed mainly of epoxy acrylate resin, monomers, and about 3–5% in weight of photo initiators. The tensile strength of the resin ranges between 36–53 MPa, as reported in the manufacturer datasheet.

The 3D printer used in this study is the masked stereolithography apparatus ELEGOO Saturn 4 Ultra LCD (Fig. 1a). A transparent LCD screen masks UV LED lights to selectively cure the resin layers. The resin hardens in correspondence of the unmasked areas of the LCD screen, due to the passage through it of the UV light; thus, the part of the object in the layer is obtained. This process is repeated layer by layer until the whole component is obtained: as a layer is completed, the build platform lifts from the resin tank with a height equal to the thickness of the subsequent layer to allow the liquid resin to cover it. Each layer is characterized by high accuracy due to the ability of the projector to quickly illuminate complex areas. After the printing process is completed, the part is removed for the subsequent post-printing phases, that are curing and washing processes. The parts are washed using an isopropyl alcohol solvent for five minutes, to remove any residues of uncured resin, and then post-cured by means of UV lights for five minutes using the dedicated washing and curing machines ELEGOO Mercury X Bundle (Fig. 1b). In this study, the curing and washing parameters were considered constant (Table 1). The Bottom Exposure Time is the exposure time to UV light of the lower part of the component, which is in contact with the printing plate. Generally, this value is higher than the ET of the subsequent layers to prevent the specimen from detaching from the printing plate. The Bottom Layer is the number of layers which constitute the lower part of the component, thus the first layers realized.

Table 1 Values of post – printing parameters

Post-printing parameters	Value	Unit
Bottom Exposure Time	40	s
Bottom Layer	5	-
Washing Time	5	min
Post Curing Time	5	min

2.2 Design of experiments

To obtain an exhaustive and efficient evaluation of the mechanical properties of the translucent LCD photocurable resin as a function of the process parameters, a Box-Behnken Design (BBD) algorithm, created by means



Fig. 1 (**a**) 3D printer, and (**b**) washing and post-curing machines

Elegoo Saturn 4 Ultra **Elegoo Mercury X - Bundle**

Table 2 Process parameter values associated with the different levels in Box-Behnken design

		Levels		
Parameters	**Units**	**Low (−1)**	**Medium (0)**	**High (1)**
Exposure Time (ET)	s	4	8	12
Layer Thickness (LT)	mm	0.01	0.05	0.09
Led Intensity (LI)	%	50	75	100

Minitab software, was used for the Design of Experiments. BBD is considered a rotatable design of the second order based on three factorial levels. The Box-Behnken Design was preferred over full factorial and Central Composite Designs because it provides a quadratic response surface with a reduced number of experimental runs while avoiding extreme parameter combinations that may generate unstable curing conditions in MSLA processes. Likewise, nonlinear multiple regression was adopted because the photopolymerization process inherently exhibits nonlinear relationships between printing parameters and mechanical response.

In the present investigation, the three process parameters taken into account are the Exposure Time (ET), Layer Thickness (LT), and Led Intensity (LI). For each parameter, three different levels were taken into account: low, medium, and high levels. Table 2 reports the values associated with the different levels. The parameter ranges investigated were selected according to the operating window recommended by the printer and resin manufacturers and validated through preliminary printing trials to ensure successful fabrication. The remaining process parameters were maintained constant to isolate the influence of exposure time, layer thickness and LED intensity.

According to the BBD methodology, 15 runs of experiments, which correspond to 15 printing processes realized with different combinations of the three selected process parameters, were necessary to obtain valuable results (Table 3).

Moreover, a non-linear multiple regression which used the least-squares method was considered to retrieve the Elastic Modulus (E), Ultimate Tensile Strength (UTS), Ultimate Flexural Strength (UFS) and the energy consumption as function of LT, ET and LI:

$$y = f(x_1, x_2, \ldots, x_n) \tag{1}$$

in which x_1, x_2, …, x_n represent input and output variables, respectively.

The goal is to find the best-fitting curve that minimizes the sum of squares of the intermediate residuals between the observed and predicted values. A model based on the following second-order Eq. (2) is used to explain the relation:

$$y = b_0 + \sum_{i=1}^{m} b_i x_i + \sum_{i=1}^{m-1} \sum_{j\geq 1}^{m} b_{ij} x_i x_j + \sum_{i=1}^{m} b_{ii} x_i^2 + \varepsilon \tag{2}$$

in which i is the linear coefficient, j the second order coefficient, b the regression coefficient, m the number of parameters, and ε the error identified on the response.

This method is generally used to predict dependent variables as a function of independent ones. Specifically, in this study, the mechanical properties of specimens under tensile and flexural conditions, and energy consumption during printing were predicted using Minitab software to perform a multiple regression analysis. In order to compare the analytical model and the experimental results, and to evaluate the model predictive capability, the R-squared (R^2) (Eq. 3), and Mean Absolute Percentage Error (MAPE) (Eq. 4) were evaluated, and the residual plots were observed. R^2

Table 3 Runs of experiments investigated, according to the Box Behnken design

Run no	Actual level of variables			Coded level of variables		
	ET [s]	LT [mm]	LI [%]	ET	LT	LI
1	12	0.09	75	1	1	0
2	12	0.05	100	1	0	1
3	8	0.09	100	0	1	1
4	8	0.05	75	0	0	0
5	4	0.05	50	−1	0	−1
6	4	0.09	75	−1	1	0
7	8	0.05	75	0	0	0
8	12	0.05	50	1	0	−1
9	4	0.05	100	−1	0	1
10	8	0.09	50	0	1	−1
11	12	0.01	75	1	−1	0
12	4	0.01	75	−1	−1	0
13	8	0.05	75	0	0	0
14	8	0.01	50	0	−1	−1
15	8	0.01	100	0	−1	1

indicates how well the model fits the experimental data, representing the proportion of variance in the dependent variable, explained by the independent variables, while MAPE is the accuracy of the predictive model. The residual plot is a diagnostic tool that measures and visualizes the residuals of a statistical model, that is the discrepancy between the observed values and the predicted ones. This adjustment helps prevent overestimation of model accuracy, particularly in complex models with several independent variables.

$$R^2 = 1 - \frac{\sum (y_i - x_i)^2}{\sum (y_i - z_i)^2} \tag{3}$$

$$MAPE = \frac{1}{n} \sum_{i=1}^{n} \left| \frac{y_i - x_i}{y_i} \right| \tag{4}$$

in which y_i is the experimental value, x_i is the predicted value, z_i is the mean of experimental values, and n is the total number of experiments.

2.3 Tensile and flexural tests

In order to evaluate the mechanical properties of the resin at different printing parameters, tensile and flexural tests were carried out at room temperature according to the ASTM D638-22 and ASTM D790-17 standards, respectively. To this purpose, tensile and flexural specimens were printed with different layer thickness (LT) values, build orientations and exposure times.

Table 3 summarizes the different printing conditions investigated in the present research, obtained by combining the different process parameters according to the BBD methodology. Five tensile and five flexural specimens were realized for each printing condition, to ensure the repeatability of the results. The reported mechanical properties correspond to the average values obtained from the five tested specimens for each condition, thereby reducing the influence of experimental variability. Dog bone tensile specimens (Type IV specimens) were realized according to the ASTM D638-22 standard for plastic samples. The tensile tests were performed using the MTS 810® universal servo-hydraulic testing machine, equipped with a 25 kN load cell. A constant crosshead speed of 5 mm/min was imposed. The strain along the loading direction was recorded during the test using an extensometer. Tensile stress vs. tensile strain curves were plotted by load and strain values. Then, the Ultimate Tensile Strength (UTS) and tensile elastic modulus (E_t) were measured as a function of the different process parameters.

As far as the flexural properties of the resin are concerned, flexural tests were performed according to the ASTM D790-17 standard for both plastics and reinforced plastics. To this purpose, samples, 127 mm in length, 12.7 mm in width and 3.2 mm in thickness, were subjected to the three-points bending tests, carried out until sample failure. A specific equipment, consisting of three cylinders with a diameter of 5.0 ± 0.1 mm, was used to perform the flexural tests. According to the standard, the support span was defined by considering a span-to-thickness ratio of 16:1. A crosshead speed of 2 mm/min was imposed. The flexural tests allowed the evaluation of the Ultimate Flexural Strength (UFS) and the flexural elastic modulus (E_f) as a function of the process parameters.

In order to evaluate the environmental footprint of the MSLA as a function of the process parameters investigated, the energy consumptions of the 3D printing process for the realization of both tensile and flexural specimens at different parameters, also including the washing and curing operations, were measured by means of a power meter inserted between the socket and the machines to assure primary data, that is directly measured, for the life cycle analysis, that is described in the next Sect. 2.4.

2.4 Life cycle assessment

The environmental footprint of the stereolithography 3D printed parts was evaluated by means of Life Cycle Assessment (LCA) methodology. The UNI ISO 14040–44 standards were followed to perform the analysis, which considers four main phases: Goal and scope definition; Life Cycle Inventory (LCI); Life Cycle Impact Assessment (LCIA) and the Interpretation of results.

2.4.1 Goal and scope definition

The present analysis aims at quantifying the environmental impacts associated with the MSLA 3D printed parts as a function of different process parameters. Specifically, the analysis was conducted for all the conditions investigated (Table 3). The functional unit (FU) was defined as the production of five specimens realized with MSLA technology. Two scenarios were investigated: in Scenario 1, FU is the production of five tensile specimens characterized by shape and dimensions according to ASTM D638-22, while in Scenario 2, FU is the production of five flexural specimens with geometry consistent with ASTM D790-17 (Sect. 2.3). Since the focus of this study is to identify which is the optimal printing parameters combination which involves high mechanical performance and low environmental impacts, a “from cradle to gate” approach was considered for both scenarios. Therefore, the material and the production process were the phases included within the system boundaries.

2.4.1.1 Life cycle inventory (LCI) The LCI represents the most relevant phase of an LCA analysis as all the necessaries data are collected to perform a valuable analysis.

As far as the material phase is concerned, as reported in Sect. 2.1, a commercial translucent photocurable resin was considered to realize the specimens. The resin production was modelled according to Bianchi et al. [1] and Mele et al. [30] that consider a composition of about 97% of monomers and oligomers (Methyl Acrylate, MA), and about 3% of photo-initiators (Methylene Diphenyl Diisocyanate, MDD) [1, 25].

The production process includes the printing process, followed by washing and post-curing operations, thus the present analysis considers the energy consumption related to all these phases. Irrespective of the printing condition investigated, the washing phase is carried out using 1 L of isopropyl alcohol. Therefore, it was not considered in the analysis as it provides the same contribution to all printing conditions of both scenarios.

Table 4 summarizes all collected data: the weight is related to one specimen; thus it was then multiplied five times to obtain the quantity of material needed to realize all specimens. The energy consumption, directly measured by a power meter as reported in Sect. 2.3, is related to the whole production process.

2.4.1.2 Life cycle impact assessment (LCIA) The LCIA phase was performed using the software SimaPro; according to literature studies on LCA [26–28], Global Warming Potential (GWP) was identified as a good representative impact category to provide an overview of the environmental footprint of both scenarios. The GWP impact category provides results in terms of kg CO_2 eq.

In this phase, an in-depth study was performed to achieve the target of the analysis, namely, to identify the best trade-off between the environmental impacts and the mechanical properties by defining the optimal combination of printing process parameters.

To this purpose, by considering the generic mechanical property X obtained by testing samples printed using the conditions reported in Table 3 (with X equal to the UTS, UFS, E_t and E_f value), a coefficient k_X was defined as the ratio between the mean value of the mechanical property X, and the environmental impacts associated to the printing condition investigated, in terms of kg CO_2 eq. Specifically, the four different coefficients k_{UTS}, k_{UFS}, k_{Et} and k_{Ef} were obtained by using the following Eqs. (5)-(8):

$$k_{UTS} = \frac{UTS}{kgCO_2eq} \tag{5}$$

Table 4 LCI of scenario 1 and scenario 2

Printing condition		Scenario 1 (Tensile specimens)		Scenario 2 (Flexural specimens)	
		Material	Production	Material	Production
		Weight/specimen [g]	Energy consumption [kWh]	Weight/specimen [g]	Energy consumption [kWh]
1	12 s 0.09 mm 75%	6.30	0.033	6.21	0.032
2	12 s 0.05 mm 100%	6.49	0.053	6.35	0.049
3	8 s 0.09 mm 100%	6.30	0.034	6.15	0.039
4	8 s 0.05 mm 75%	6.35	0.040	6.28	0.037
5	4 s 0.05 mm 50%	6.16	0.032	6.38	0.029
6	4 s 0.09 mm 75%	6.30	0.028	6.00	0.027
7	8 s 0.05 mm 75%	6.40	0.039	6.29	0.025
8	12 s 0.05 mm 50%	6.30	0.043	6.20	0.042
9	4 s 0.05 mm 100%	6.30	0.038	5.95	0.035
10	8 s 0.09 mm 50%	6.23	0.027	6.90	0.027
11	12 s 0.01 mm 75%	10.37	0.144	9.07	0.138
12	4 s 0.01 mm 75%	10.30	0.078	9.68	0.094
13	8 s 0.05 mm 75%	6.19	0.039	6.28	0.039
14	8 s 0.01 mm 50%	10.66	0.094	10.07	0.09
15	8 s 0.01 mm 100%	10.57	0.126	9.44	0.124

$$k_{UFS} = \frac{UFS}{kgCO_2eq} \tag{6}$$

$$k_{Et} = \frac{Et}{kgCO_2eq} \tag{7}$$

$$k_{Ef} = \frac{Ef}{kgCO_2eq} \quad (8)$$

These coefficients have the same unit of measurement, i.e. GPa/kg CO_2 eq. In this way, the printing condition characterized by the highest k_X value represents the optimal solution that simultaneously maximizes the considered mechanical property X while reducing the environmental impact associated.

3 Results and discussions

3.1 Tensile and flexural tests

In order to evaluate the effect of layer thickness, exposure time, and led intensity on the mechanical properties of MSLA-printed parts, tensile and flexural specimens were printed at different conditions and then tested at room temperature. Furthermore, energy consumption during the printing process was measured for each condition to analyze the influence of LT, ET and LI.

Typical tensile stress vs. tensile strain curves, obtained at different MSLA printing conditions, were shown in Fig. 2. Irrespective of the printing parameters, the tensile stress linearly increases with strain in the elastic region until yielding; then, the stress further rises with a non-linear behaviour up to a peak value (UTS). Depending on the process parameters, the peak of the curve can correspond to the fracture of the material or to the onset of necking. In the latter case, the stress tends to decrease with increasing strain until the specimen failure.

It can be observed that the process parameters affect the mechanical properties of the MSLA printed specimens. As far as the effect of layer thickness is concerned, for a given strain value in percentage, the tensile strength and ductility increase with decreasing LT value. Such behaviour can be attributed to the more effectiveness of the curing process and to the improved interlayer adhesion as low layer thicknesses are printed (Fig. 2a).

The strength levels of the tensile specimens can be further enhanced by increasing the exposure time. Such improvement can be attributed to the extended curing process and the higher amount of energy delivered to each layer, which promote a higher degree of polymerization and crosslinking density for a given thickness value. However, the increase in ET value leads to a decrease in ductility: as the crosslinking density rises, the material becomes stiffer and less capable of plastic deformation before fracture. As a consequence, a more complete polymerization leads to increased material brittleness (Fig. 2b).

Furthermore, as far as the effect of led intensity is concerned, higher irradiation levels promote deeper light penetration and a more complete polymer crosslinking within the resin. This results in increased tensile strength levels, improved ductility, and enhanced dimensional stability. On the contrary, lower LI values limit the depth of cure and reduce the degree of polymerization, leading to partially uncured regions that compromise the mechanical performance and the load-bearing capacity (Fig. 2b).

Figure 3 shows typical flexural stress vs. flexural strain curves obtained by MSLA printed specimens at different MSLA process parameters, subjected to the three-point

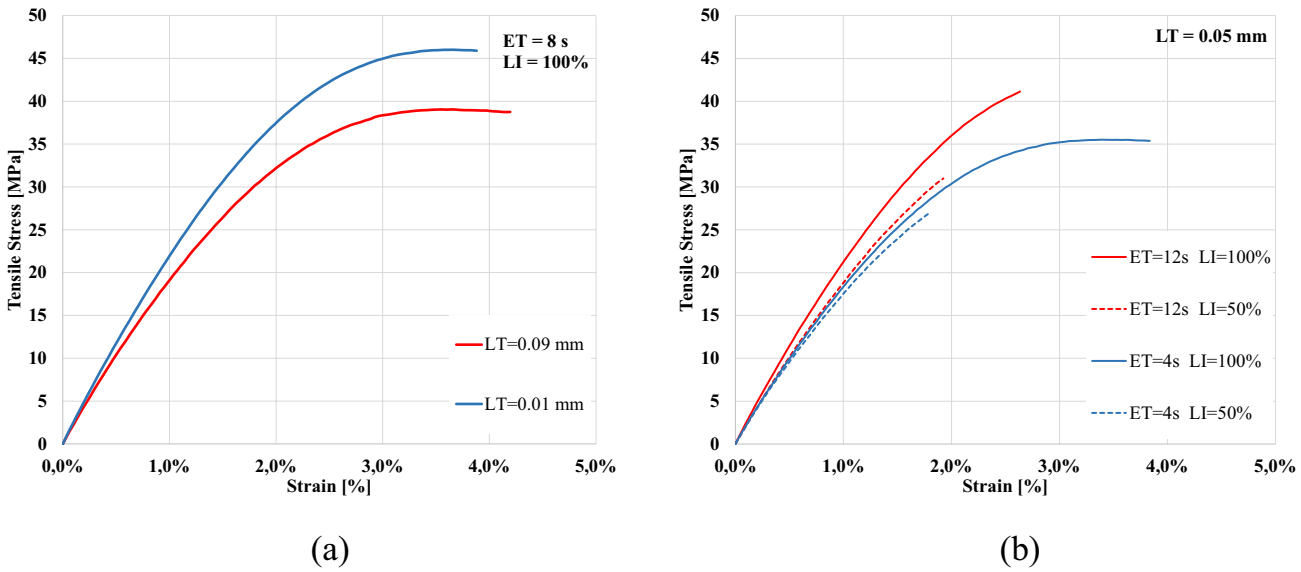

Fig. 2 Typical tensile stress vs. tensile strain curves obtained by specimens MSLA printed at different printing conditions: (**a**) effect of LT and (**b**) effect of ET and LI

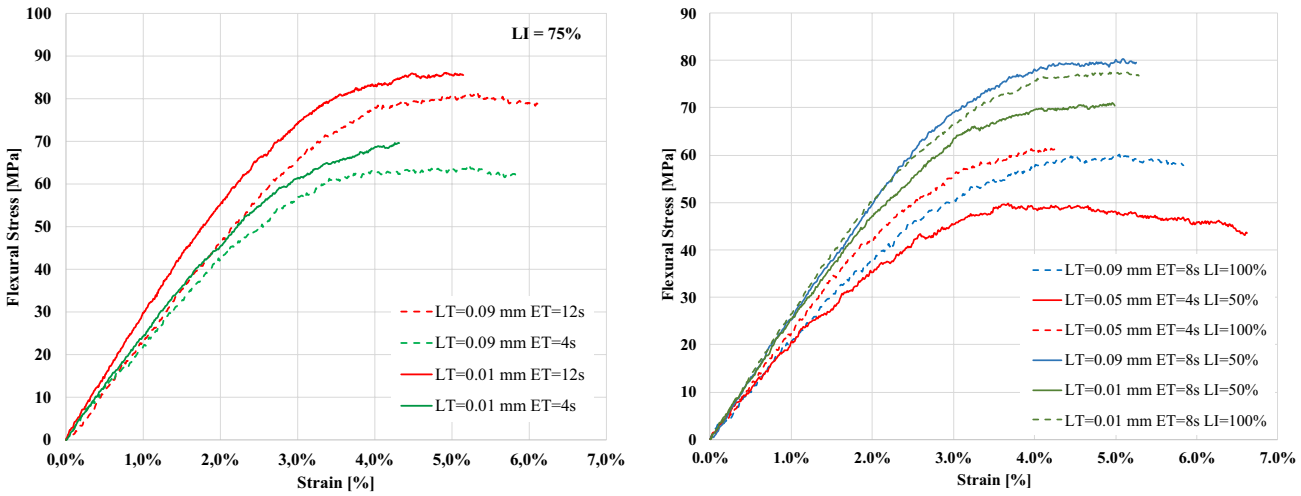

Fig. 3 Typical flexural stress vs. flexural strain curves obtained by specimens MSLA printed at different printing conditions: (**a**) effect of LT and ET, and (**b**) effect of LT, ET and LI

bending test. It can be observed that the curves are characterized by an increase in flexural stress with increasing flexural strain until reaching a peak value in which the specimen fracture occurs.

Consistent with the tensile results shown in Fig. 2, the specimens realized using the thinnest layer thickness investigated (LT = 0.01 mm) exhibit high flexural strength and poor ductility, indicating a homogeneous and effective polymerization process. As a matter of fact, for thin layers, light can penetrate the entire layer effectively, promoting uniform curing and strong interlayer adhesion. On the contrary, as the layer thickness increases (e.g., LT = 0.09 mm), the lower regions of each layer can receive insufficient energy due to limited light penetration, particularly under low-intensity or short-exposure conditions. This leads to heterogeneous polymerization, reduced interlayer bonding, and a lower cross-linking density at the interface, ultimately compromising the flexural strength and, in some cases, increasing ductility due to a less constrained polymer network (Fig. 3a).

The exposure time parameter also significantly influences the flexural behavior of the resin processed via MSLA technology. As shown in Fig. 3a, longer exposure times (e.g., ET = 12 s) result in higher flexural stress levels, indicating enhanced polymerization and strong interlayer bonding. In contrast, shorter ET values result in reduced ultimate flexural strength and premature stress drops, likely due to incomplete polymerization and suboptimal interlayer adhesion. Finally, the experimental results reported in Fig. 3b show a complex relationship between led intensity, exposure time, and layer thickness during the MSLA process, which significantly affects the flexural properties of the printed resin. Specifically, two behaviors can be observed depending on the combination of these parameters. When the led intensity was increased under conditions of prolonged exposure time and low to medium layer thickness, a reduction in flexural strength can be observed. This phenomenon can be attributed to the overcuring and excessive crosslinking, leading to an excessive dense polymer network. This overcuring may increase brittleness and reduce the material's ability to dissipate stress under bending. Furthermore, a high degree of polymerization can lead to increased volumetric shrinkage and residual stresses, potentially causing microcracks or interlayer weakening, which compromise flexural performance. Conversely, when LI value was increased under conditions of short exposure time and medium to high layer thickness, the flexural strength tends to improve, although a decrease in ductility was also noted. This behavior can be attributed to a controlled energy quantity: the high-intensity light source applied for a short duration can deliver sufficient energy to ensure proper polymerization without inducing overcuring effects, especially for thicker layers that require deeper light penetration. Furthermore, a higher led intensity can enhance curing depth and interlayer bonding, resulting in a mechanically stronger structure under flexural load.

These results demonstrate that the led intensity cannot be evaluated in isolation, but it must be considered in conjunction with exposure time and layer thickness, as the total energy input and the resulting polymerization kinetics are critical in determining the final flexural properties of MSLA-printed parts.

Table 5 summarizes the mechanical properties of tensile and flexural specimens obtained by varying the printing

Table 5 Mechanical properties of tensile and flexural specimens and energy consumptions measured during the MSLA process as a function of the different printing conditions

	Tensile specimens					Flexural Specimens				
Conditions	E_t [GPa]		UTS [MPa]		Energy consumption [KWh]	E_f [GPa]		UFS [MPa]		Energy consumption [KWh]
1	2.09	±2.12%	35.49	±4.52%	0.033	2.67	±4.28%	70.05	±4.98%	0.032
2	2.43	±2.20%	42.49	±5.15%	0.053	2.40	±4.04%	67.75	±2.33%	0.049
3	2.22	±3.45%	36.88	±4.43%	0.034	2.60	±3.89%	60.28	±4.88%	0.039
4	2.05	±1.19%	36.74	±4.99%	0.04	2.40	±3.80%	55.87	±3.61%	0.037
5	1.73	±6.21%	26.10	±4.65%	0.032	2.33	±3.93%	51.97	±5.57%	0.029
6	1.78	±1.64%	31.76	±1.19%	0.028	2.81	±4.52%	63.65	±3.80%	0.027
7	2.08	±3.40%	37.12	±2.58%	0.039	3.32	±4.39%	73.25	±3.07%	0.025
8	2.06	±2.96%	35.47	±5.01%	0.043	3.08	±3.60%	71.62	±3.32%	0.042
9	1.99	±4.84%	32.15	±3.32%	0.038	2.75	±5.66%	68.89	±5.55%	0.035
10	1.88	±3.48%	31.53	±4.09%	0.027	2.96	±5.04%	81.92	±4.30%	0.027
11	2.66	±3.85%	48.60	±4.17%	0.144	3.49	±4.99%	86.18	±1.48%	0.138
12	2.25	±6.25%	30.69	±7.24%	0.078	2.58	±3.59%	62.64	±4.85%	0.094
13	2.10	±1.62%	36.54	±2.00%	0.039	2.76	±3.65%	77.34	±2.30%	0.039
14	1.97	±4.72%	34.20	±1.42%	0.094	2.59	±3.19%	64.50	±4.84%	0.090
15	2.43	±4.01%	43.98	±4.14%	0.126	2.91	±4.31%	78.09	±2.83%	0.124

parameters. The energy consumption values measured during the MSLA process as a function of the process parameters are also reported.

Overall, the observed mechanical behaviour can be interpreted considering the balance between the energy delivered during photopolymerization and the curing depth achieved within each deposited layer. Insufficient energy input results in incomplete polymerization, limited curing depth and poor interlayer adhesion, ultimately reducing the mechanical performance of the printed parts. Conversely, excessive energy input promotes overcuring, increased cross-link density, volumetric shrinkage and residual stresses, leading to a more brittle material response. Therefore, the optimal mechanical performance is achieved under intermediate processing conditions, which maximize polymer cross-linking while avoiding the detrimental effects associated with excessive curing energy.

Overall, the mechanical trends observed in the present investigation are consistent with previous studies on MSLA photopolymerization. In particular, Valizadeh et al. [14, 15] and Temiz [12] reported that increasing the exposure time enhances the tensile properties owing to a higher degree of polymer cross-linking, while reduced layer thickness promotes stronger interlayer bonding and improved mechanical performance. Similar observations were also reported by Milovanović et al. [10] for the flexural behaviour of MSLA printed components. Therefore, the present experimental results confirm the physical mechanisms already identified in the literature.

These experimental observations also explain the nonlinear behaviour identified by the regression models presented in the following section, confirming that the interaction among exposure time, layer thickness and LED intensity governs both the curing kinetics and the final mechanical performance of MSLA printed parts.

3.2 Non-linear multiple regression

The tensile and flexural mechanical properties of MSLA printed specimens and energy consumption during printing were predicted by using a non-linear multiple regression (MR) analysis.

As far as the tensile properties are concerned, the output of the non-linear MR is represented by Eqs. 9, 10 and 11, in which the tensile elastic modulus, ultimate tensile strength and energy consumption to produce five tensile specimens are expressed as a function of ET, LT and LI. The coefficients from A1 to A6, from B1 to B6, and from E1 to E6 are the results of the MR analysis and they are reported in Appendix A.

$$E_t = A_0 \cdot ET + A_1 \cdot LT + A_2 \cdot LI + A_3 \cdot ET^2 + A_4 \cdot LT^2 + A_5 \cdot LI^2 + A_6 \cdot ET^3 \quad (9)$$

$$UTS = B_0 \cdot ET + B_1 \cdot LT + B_2 \cdot LI + B_3 \cdot ET^2 + B_4 \cdot LT^2 + B_5 \cdot LI^2 + B_6 \cdot ET^3 \quad (10)$$

$$EC_t = E_0 \cdot ET + E_1 \cdot LT + E_2 \cdot LI + E_3 \cdot ET^2 + E_4 \cdot LT^2 + E_5 \cdot LI^2 + E_6 \cdot ET^3 \quad (11)$$

The results obtained by Eq. 9 are show in Fig. 4 as tensile elastic modulus as a function of printing parameters. It can be observed that E_t tends to increase with layer thickness up to a peak value (typically reached for LT of about 0.045—0.055 mm) and then it decreases with a further increase in LT. This result can be attributed to the highly negative quadratic term associated with LT^2 (A_4=−118) in the regression model, which strongly affects the response and suggests the existence of an optimal thickness that maximizes the

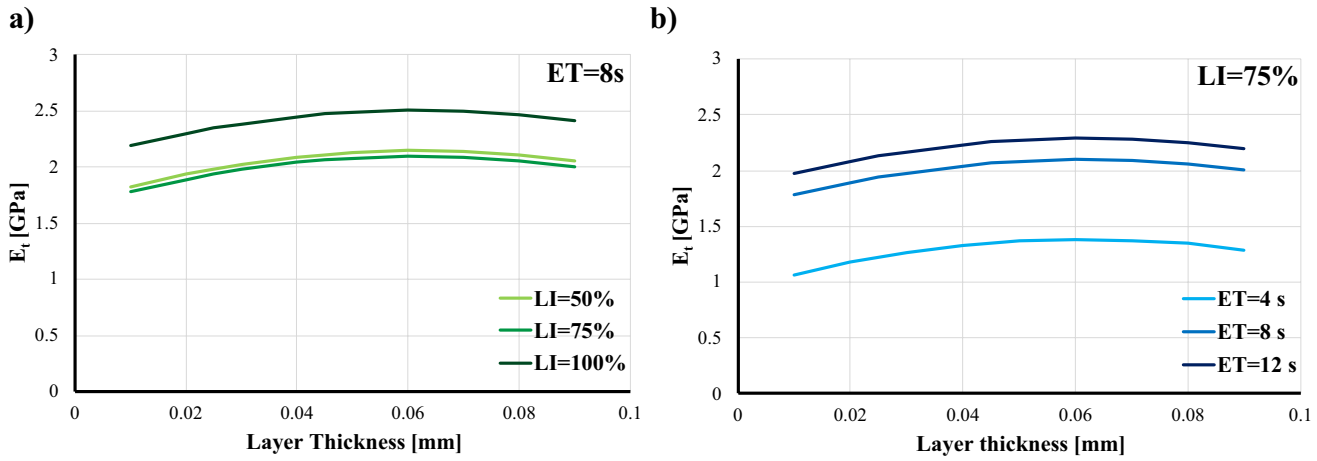

Fig. 4 Effect of (**a**) led intensity and (**b**) exposure time on the predicted tensile elastic modulus vs layer thickness curves

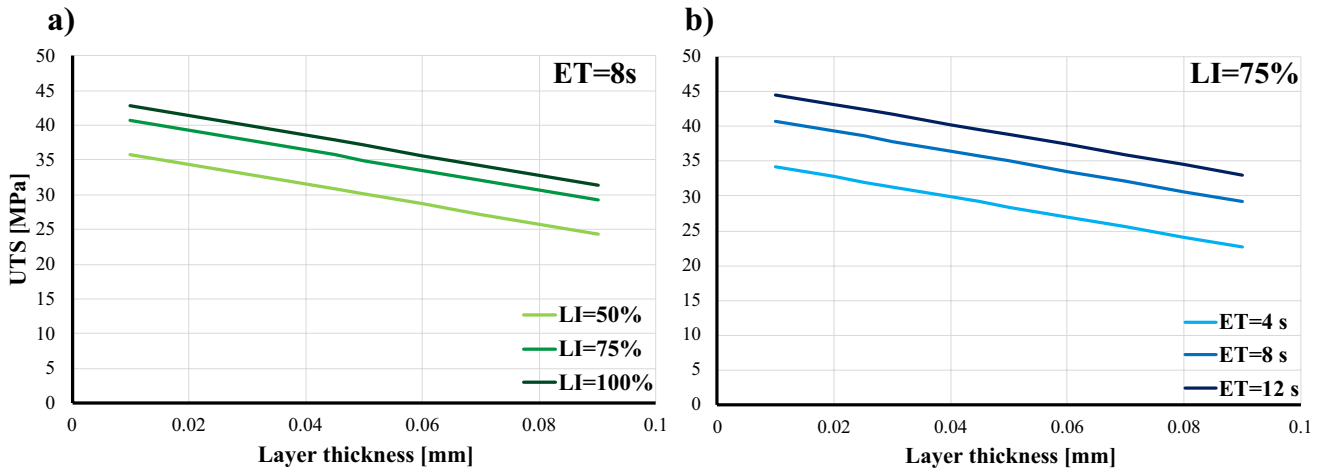

Fig. 5 Effect of (**a**) led intensity and (**b**) exposure time on the predicted ultimate tensile strength vs layer thickness curves

tensile elastic modulus. The increase in led intensity has a beneficial effect on E_t, particularly as LI increases from 75 to 100%. This trend arises from the interplay between the negative linear coefficient associated with LI ($A_2 = -4.77$) and the positive quadratic term for LI^2 ($A_5 = 3.66$). As a result, while lower LI levels may slightly reduce performance, higher intensities lead to a marked increase in E_t, as the quadratic contribution becomes dominant.

These results highlight the importance of high light exposure in achieving effective material crosslinking and curing during the process. Similarly, exposure time exhibits a nonlinear contribution to E_t. As ET increases from 4 to 8 s, the tensile elastic modulus improves, whereas a further increase to 12 s leads to a plateau or a slight decrease. This behavior reflects the competing effects of the linear ($A_0 = 0.93$) , quadratic ($A_3 = -0.092$), and cubic ($A_6 = 0.00315$) terms associated with ET in the regression model. While the positive linear and cubic terms initially promote an increase in E_t, the negative quadratic term moderates this effect, indicating diminishing returns beyond a critical exposure time threshold.

The behavior of the predicted ultimate tensile strength as a function of the main printing parameters is shown in Fig. 5, as derived from Eq. 10. Specifically, irrespective of led intensity and exposure time values considered, a consistent and nearly linear decrease in UTS is observed as layer thickness increases. This behavior is in agreement with the regression model, in which the linear term associated with LT exhibits a highly negative coefficient ($B_1 = -144$), dominating over the opposing effect of the quadratic term ($B_4 = +759$). As a result, within the considered range of LT (0.01–0.09 mm), the model predicts a monotonic decrease, indicating that thinner layers are associated with higher UTS values. As far as the effect of led intensity on UTS vs. LT curves is concerned (Fig. 5a), for a given LT, an increase in LI results in higher UTS values, consistent with the strong positive linear coefficient ($B_2 = +46.9$) in the model. However, the presence of a negative quadratic

term ($B_5 = -21.9$) indicates a non-linear relationship, with marginal gains decreasing at higher intensities. This behaviour is reflected in the smaller differences between the UTS values at LI = 75% and LI = 100%, compared with the larger difference observed between LI = 50% and 75%. In Fig. 5b Fig. 5b, exposure time exhibits a positive effect on UTS, particularly between 4 and 8 s. This trend is supported by the combination of a positive linear coefficient ($B_0 = +4.22$) and a small positive cubic term ($B_6 = +0.0088$). The trend begins to flatten between 8 and 12 s, indicating diminishing returns, which can be attributed to the negative quadratic term ($B_3 = -0.297$). Overall, longer exposure enhances tensile strength, but the benefit decreases beyond a certain threshold.

The energy consumption per tensile specimen (EC_t) was modeled as a function of the process parameters using a non-linear regression equation (Fig. 6). Based on the coefficient values, the most influential parameter on energy consumption is the layer thickness. The negative linear coefficient (E_1 = –2.88) indicates a steep reduction in energy consumption with increasing LT due to the reduction in the number of layers needed for the build. This effect dominates both subfigures. However, the positive quadratic term (E_4 =+18.80) slightly moderates this decrease at higher LT values, resulting in a progressive flattening of the curves. Exposure Time also plays a notable role. Although the linear coefficient (E_0 =+0.0495) suggests a mild increase in EC_t with longer ET, the negative quadratic (E_3= –0.00644) and positive cubic (E_1 =+0.000272) coefficients result in a non-linear effect, particularly visible in Fig. 6b. This interplay leads to diminishing returns in energy efficiency at higher exposure times. Lastly, Light Intensity has the least pronounced effect on energy consumption. The model coefficients (E_2 =+0.007; E_5=+0.013) indicate a slight increase in EC_t with increasing LI, which aligns with the trends observed in Fig. 6a, where the curves for higher light intensities consistently lie above those for lower intensities. Nevertheless, the overall influence of LI is minor compared to the other parameters.

The outputs of the non-linear MR is represented by the Eq. 12–14 for the Flexural tests, where the Flexural Elastic modulus ($E_f, [GPa]$), Ultimate Flexural Strength ($UFS[MPa]$), and Energy consumption ($EC_f, [KWh]$) to produce 5 flexural specimens are expressed as a function of exposure time, layer thickness, and led intensity. The coefficient D1-D6, E1-E6, and F1-F6, reported in Appendix A, are the results of the MR analysis.

$$E_f = C_0 \cdot ET + C_1 \cdot LT + C_2 \cdot LI + C_3 \cdot ET^2 + C_4 \cdot LT^2 + C_5 \cdot LI^2 + C_6 \cdot ET^3 \quad (12)$$

$$UFS = D_0 \cdot ET + D_1 \cdot LT + D_2 \cdot LI + D_3 \cdot ET^2 + D_4 \cdot LT^2 + D_5 \cdot LI^2 + D_6 \cdot ET^3 \quad (13)$$

$$EC_f = F_0 \cdot ET + F_1 \cdot LT + F_2 \cdot LI + F_3 \cdot ET^2 + F_4 \cdot LT^2 + F_5 \cdot LI^2 + F_6 \cdot ET^3 \quad (14)$$

Figure 7 shows the effect of the exposure time and led intensity on the elastic flexural modulus vs. layer thickness curves predicted by the non-linear regression model.

The analysis of the regression coefficients indicates that layer thickness has the most pronounced influence on E_f. The negative linear term (C_1 = –7.3) suggests a reduction in stiffness with increasing LT, which is consistent with the downward trends observed in both Fig. 7a and Fig. 7b. However, the positive quadratic coefficient (C_4 =+57) reveals a non-linear behavior, leading to a shallow minimum at intermediate LT values, beyond which the decrease in modulus slows or slightly reverses. Exposure time also significantly affects the flexural modulus. The positive linear coefficient (C_0=+0.691) and negative quadratic term (C_3 = –0.087), combined with a small positive cubic term (C_6 =+0.00352), describe a non-monotonic relationship. As shown in Fig. 7b, increasing ET generally enhances the modulus; however, the rate of improvement progressively decreases at longer ET, indicating a plateau or saturation effect. Light intensity

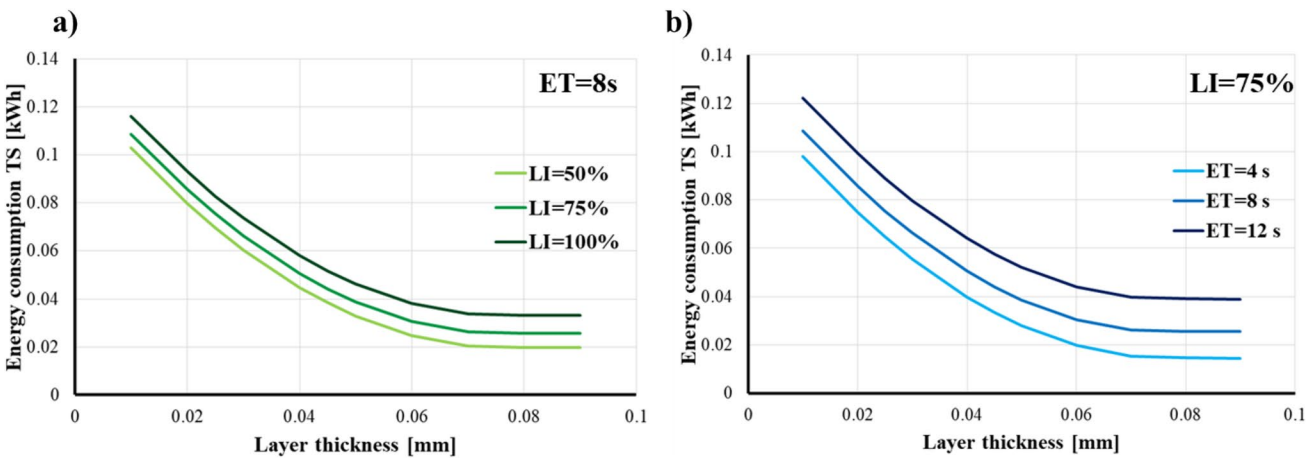

Fig. 6 Effect of (**a**) led intensity and (**b**) exposure time on the predicted energy consumption vs layer thickness curves

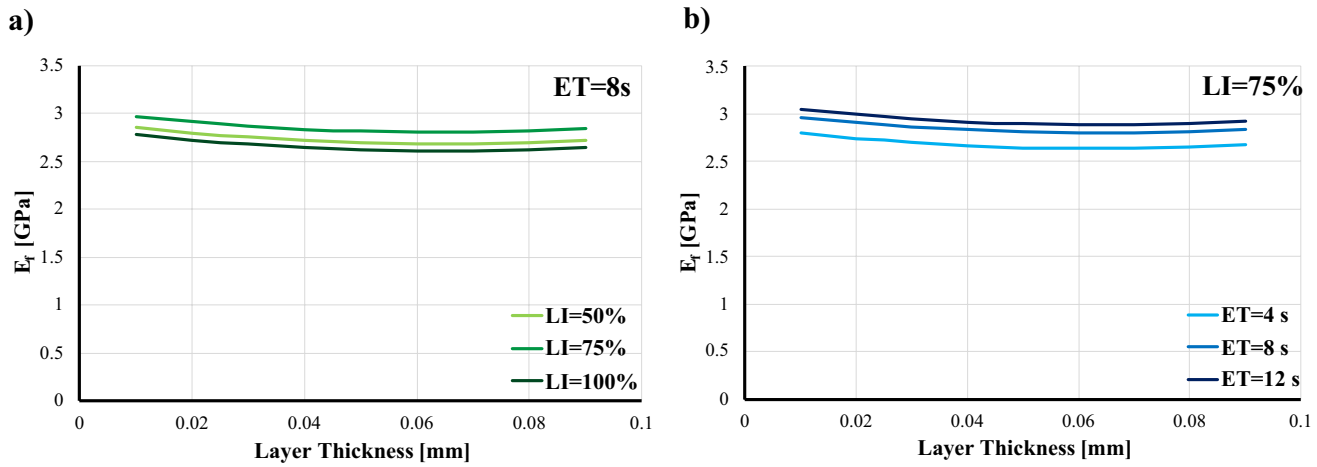

Fig. 7 Effect of (**a**) led intensity and (**b**) exposure time on the predicted elastic flexural modulus vs. layer thickness curves

has a moderate positive influence on E_f, as indicated in the positive linear coefficient (C_2 =+3.54). Nevertheless, the negative quadratic term (C_5 = –2.46) points to diminishing returns at higher intensities. This behavior is shown in Fig. 7a, by the slight but consistent upward shift of the curves from LI=50% to LI=100%, suggesting that higher light intensity promotes polymerization and cross-linking, thereby enhancing the stiffness of the printed material.

Figure 8 shows the predicted UFS as a function of layer thickness at different light intensity levels (Fig. 8a) and exposure times (Fig. 8b). It can be observed that UFS initially decreases as LT increases up to approximately 0.06 mm, then slightly increases to LT=0.09 mm. This non-linear relationship is consistent with the model coefficients, which show a strong negative linear term (D_1 = −297) balanced by a substantial positive quadratic term (D_4 =+2484). These terms generate the observed U-shaped trend, where both very thin and relatively thick layers yield slightly higher strength values than intermediate thicknesses. In Fig. 8a, higher LI values consistently produce greater UFS across all layer thicknesses, with 100% LI producing the highest strength values. This positive correlation corresponds to the model positive linear coefficient for LI (D_2 =+41.00). However, the reduced difference between the curves at higher intensity levels reflects the negative quadratic term (D_5 = −25.50) that indicates diminishing returns at higher intensity values.

Figure 8b shows that increasing exposure time leads to higher UFS values. This behaviour is supported by the strong positive linear coefficient for ET (D_0 =+22.2). The smaller gap between the 8 s and 12 s curves, compared with that between 4 and 8 s, corresponds to the negative quadratic term (D_3 = −2.66), suggesting decreasing marginal benefits. However, the small positive cubic term (D_6 =+0.105) indicates a potential complex relationship at extended exposure times.

The energy consumption for the realization of five flexural specimens (EC_f) was modeled as a function of process parameters using a non-linear regression equation (Fig. 9). It can be observed that EC_f—LT curves are characterized

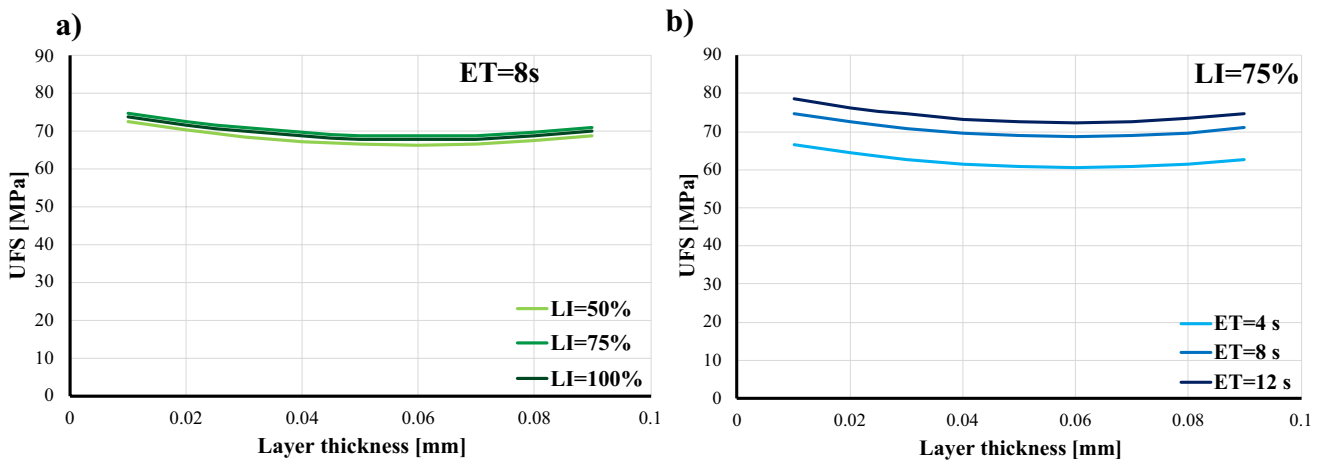

Fig. 8 Effect of (**a**) led intensity and (**b**) exposure time on the predicted UFS vs. LT curves

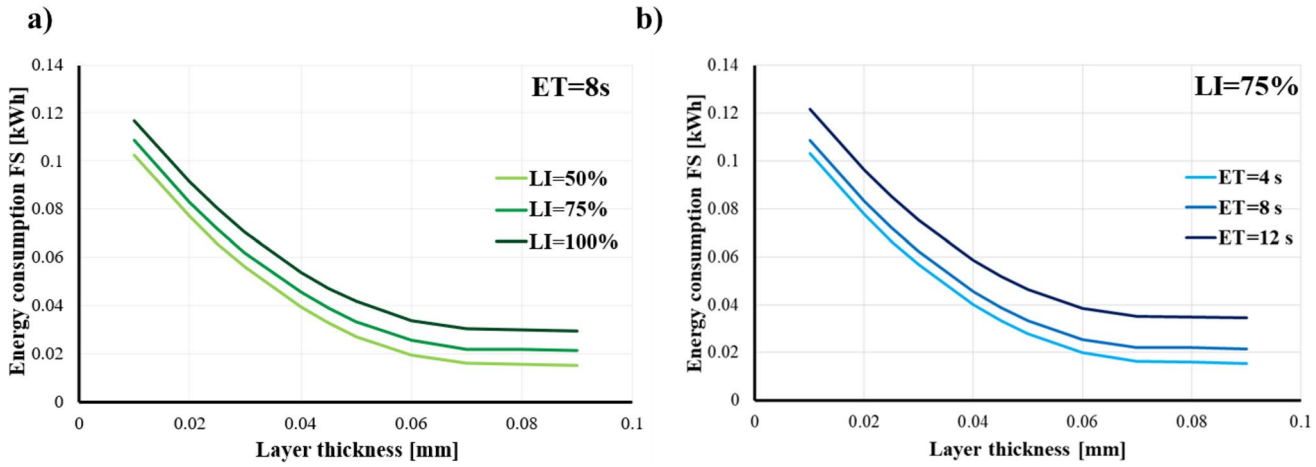

Fig. 9 Effect of (**a**) led intensity and (**b**) exposure time on the predicted flexural energy consumption vs. layer thickness curves

by the same trend exhibited by the EC_t – LT curves (Fig. 6). As a matter of fact, energy consumption decreases with increasing layer thickness, and decreasing both LED intensity (Fig. 9a) and exposure time (Fig. 9b).

To assess the quality of the developed regression models for mechanical properties and energy consumption, a comprehensive statistical analysis was performed, by considering the coefficient of determination (R^2), Mean Absolute Percentage Error (MAPE), and residual distributions. In an ideal model, the R^2 and MAPE values would be equal to 100% and 0%, respectively. The residuals should be randomly scattered around zero, with no visible patterns or trends. This randomness suggests that the model has captured the underlying structure of the data and that the errors are purely random. The closer the values of these fit indicators are to the ideal values, the better the model fits the data.

As far as the developed mathematical model is concerned, Table 6 summarizes the R^2 and MAPE values, whilst Fig. 10 shows the residual plots.

The model developed to predict the tensile modulus (Eq. 9) achieved a coefficient of determination equal to 96.45%, demonstrating an excellent agreement between the predicted values and the corresponding experimental results. This high R^2 value indicates that the model can capture the relationship between the input variables and the tensile modulus with a high degree of reliability. Furthermore, the MAPE of 4.00% highlights the strong predictive performance of the model, confirming that the average deviation between predicted and experimental values is very low. This value of MAPE is generally considered well within acceptable limits, thereby supporting the robustness and practical applicability of the proposed predictive approach. In particular, the combined statistical indicators suggest that the model provides accurate and consistent estimations of the tensile modulus, making it suitable for engineering analysis, design optimization, and performance evaluation tasks. As shown in Fig. 10a, the corresponding residual plot shows a random distribution around the zero line, with no observable pattern or systematic error, supporting the validity of the model and lack of bias. The UTS predictive model (Eq. 10) exhibits the highest R^2 value among the developed models, equal to 99.71%, with a very low mean absolute percentage error of 2.07%, demonstrating an excellent level of agreement between the predicted and experimentally UTS values, and, consequently, confirming the high model predictive capability. Despite the high level of accuracy, the residual analysis, shown in Fig. 10b, displays a slight funnel-shaped pattern, characterized by an increase in residual variance at higher UTS values. This behavior can be attributed to the presence of a poor heteroscedasticity, that is the variability of the prediction error is not entirely constant across the full range of the response variable. However, the residuals remain symmetrically distributed around zero, with no evident systematic trends or curvature. This confirms the absence of significant model bias and indicates that the predictive capability remains stable and reliable throughout the range investigated. Overall, although a minor heteroscedastic effect can be observed at higher UTS values, its magnitude appears limited and does not substantially compromise the robustness of the proposed model.

As far as the energy consumption model for tensile specimens is concerned (Eq. 11), a solid R^2 value of 97.90% and a

Table 6 R-squared and MAPE for mathematical models

	Equation	R^2 [%]	MAPE [%]
E_t	(9)	96.45	4.00
UTS	(10)	99.71	2.07
EC_t	(11)	97.90	6.89
E_f	(12)	98.98	4.11
UFS	(13)	98.80	4.47
EC_f	(14)	98.60	7.47

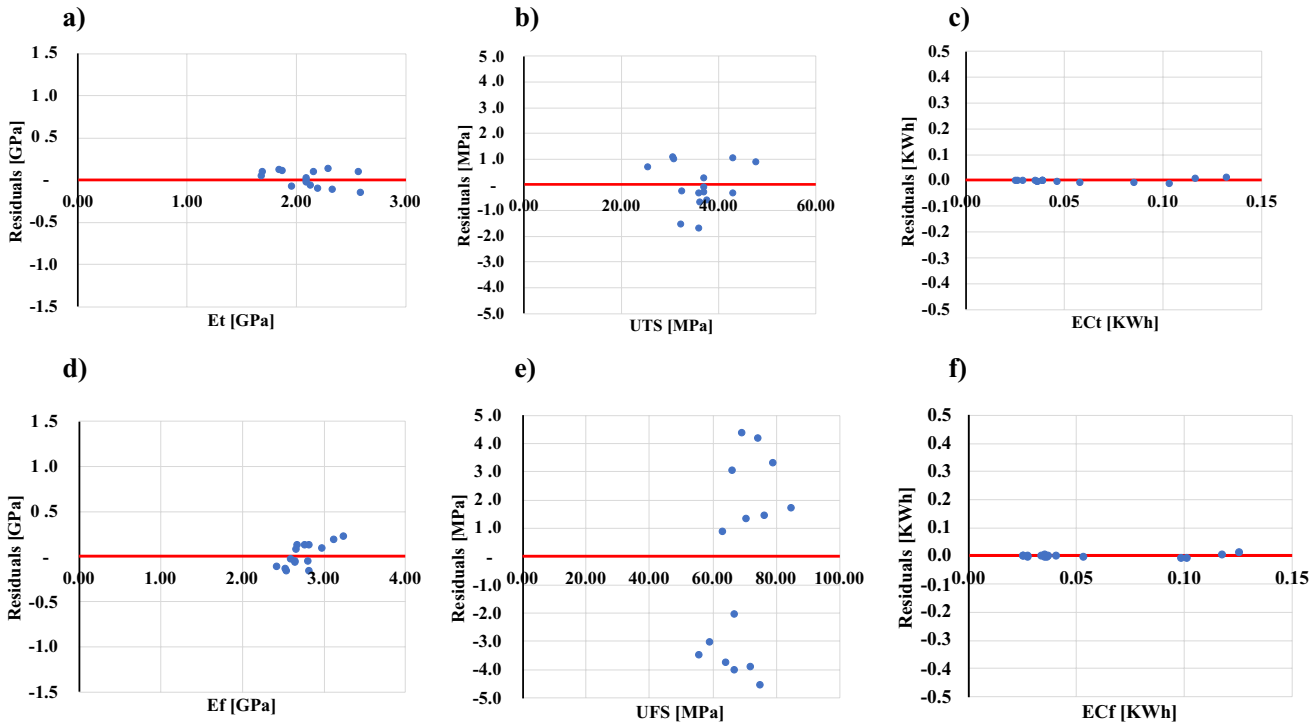

Fig. 10 Residual plots for the obtained mathematical models

MAPE of 6.89% are obtained, demonstrating the strong predictive capability of the model. Although the MAPE value is slightly higher than that observed for the tensile property models, it remains within acceptable engineering limits, particularly considering the inherently higher variability associated with energy-related measurements. Energy consumption is typically influenced by multiple interacting factors, including machine dynamics and material response, which can introduce additional dispersion in the data. The residual plot shown in Fig. 10c does not exhibit any evident systematic pattern, and the residuals are tightly clustered around the zero line. This behavior indicates that the model provides stable and reliable predictions in the investigated range.

The model developed for the flexural modulus (Eq. 12) achieved an R^2 of 98.98% and MAPE of 4.11%, indicating both high explanatory power and strong predictive accuracy. The residuals are evenly distributed with limited dispersion and no discernible trend, suggesting that the model effectively captures the relationship between the parameters and the flexural stiffness (Fig. 10d).

For the ultimate flexural strength model (Eq. 13), the predictive performance remains very strong, confirmed by the R^2 of 98.80% and MAPE 4.47%. However, as shown in Fig. 10e, the residual analysis reveals a more pronounced curvature as compared to the previous models, characterized by relatively higher residuals at both low and high strength values. This pattern can be attributed to the slight underfitting of the extremes of the response variable, suggesting that the formulation of the current model does not fully capture nonlinear effects at the boundaries of the experimental range. Nonetheless, the overall predictive accuracy remains high and suitable for practical engineering applications. Finally, the energy consumption model for flexural testing (Eq. 14) achieved an R^2 value of 98.60% with a MAPE of 7.47%, representing the highest prediction error among the developed models, but still within acceptable limits for engineering purposes. The residuals, shown in Fig. 10f, appear reasonably homoscedastic and centered around zero, although minor deviations from symmetry can be observed. These slight irregularities can be attributed to unmodeled factors influencing the energy consumption process, such as small fluctuations in machine efficiency, variations in testing speed, or ambient environmental conditions. Despite these minor deviations, the statistical metrics and residual distribution confirm the robustness and reliability of the proposed model.

3.3 Interpretation of LCA results

As far as energy consumption is concerned, Sect. 3.2. shows a good fitting between the values obtained by the analytical model and those directly measured with the power meter, for both tensile and flexural specimens. Thus, the LCA analysis was performed by considering the values directly measured.

As reported in Sects. 2.4.1. and 2.4.3., the aim of this analysis is to identify which is the printing condition which represents the best trade-off between the mechanical properties and the environmental impacts. This evaluation was performed for all the investigated mechanical properties (UTS, UFS, E_t and E_f), by considering the k coefficient defined in Sect. 2.4.3.

Table 7 reports the LCA analysis results according to GWP methodology; in particular, the environmental footprint related to the material and production phases of both investigated scenarios are highlighted.

The total environmental load is similar between the two analyzed scenarios: these values vary within a range of about ± 10%, except for the printing condition n. 15, in which the impacts of Scenario 2 are lower than those of Scenario 1 of about 12%.

As a general outcome, the material phase results as the most impactful one: it represents about 78–92% and 77–93% of the total ecological footprint for Scenario 1 and Scenario 2, respectively.

The printing conditions numbers 11, 12, 14 and 15 show the highest environmental impacts for both scenarios. This

Table 7 GWP results of scenario 1 and scenario 2 phases

		Scenario 1 [kg CO_2 eq]			Scenario 2 [kg CO_2 eq]		
Printing condition		Material	Production	Total	Material	Production	Total
1	12 s 0.09 mm 75%	0.1213	0.0126	0.1339	0.1195	0.0122	0.1318
2	12 s 0.05 mm 100%	0.1249	0.0202	0.1452	0.1222	0.0187	0.1410
3	8 s 0.09 mm 100%	0.1213	0.0130	0.1343	0.1184	0.0149	0.1333
4	8 s 0.05 mm 75%	0.1222	0.0153	0.1375	0.1209	0.0141	0.1350
5	4 s 0.05 mm 50%	0.1186	0.0122	0.1308	0.1228	0.0111	0.1339
6	4 s 0.09 mm 75%	0.1213	0.0107	0.1320	0.1155	0.0103	0.1258
7	8 s 0.05 mm 75%	0.1232	0.0149	0.1381	0.1211	0.0096	0.1306
8	12 s 0.05 mm 50%	0.1213	0.0164	0.1377	0.1194	0.0160	0.1354
9	4 s 0.05 mm 100%	0.1213	0.0145	0.1358	0.1145	0.0134	0.1279
10	8 s 0.09 mm 50%	0.1199	0.0103	0.1302	0.1328	0.0103	0.1431
11	12 s 0.01 mm 75%	0.1996	0.0550	0.2546	0.1746	0.0527	0.2273
12	4 s 0.01 mm 75%	0.1983	0.0298	0.2281	0.1863	0.0359	0.2222
13	8 s 0.05 mm 75%	0.1192	0.0149	0.1341	0.1209	0.0149	0.1358
14	8 s 0.01 mm 50%	0.2052	0.0359	0.2411	0.1938	0.0344	0.2282
15	8 s 0.01 mm 100%	0.2035	0.0481	0.2516	0.1817	0.0474	0.2291

result is related to the low value of layer thickness (0.01 mm) considered for these printing conditions, which involves an increase in the total printing time. Moreover, as stated in Sect. 2.4.2., the weight of the specimens is higher than that of specimens realized with other printing conditions and, consequently, a higher quantity of material is required. In addition, the increase in the total printing time results in a higher quantity of energy consumed during the printing process. Thes two factors lead to an increase of the environmental impacts with respect to the other printing conditions, for both the analyzed scenarios.

Figure 11 reports the environmental impacts of all the printing conditions considered of both analyzed scenarios in terms of kg CO_2 eq and the trend of the mechanical properties investigated. In particular, Fig. 11a shows the relation between the ecological footprint and the UTS and UFS; whilst Fig. 11b highlights the correlation between the environmental footprint and the E_t and E_f.

The blue line represented in Fig. 11a shows the UTS trend: it varies within a range between about 26–49 MPa, with highest values reached by specimens realized with printing conditions number 2, 11 and 15. To identify the best trade-off between the UTS and the environmental impacts, a particular focus is given to those of Scenario 1 for these three printing conditions. The ecological footprint of printing condition 2 is relevantly lower than those of printing conditions 11 and 15; thus, the first one could represent the best compromise alternative for application in which high tensile performances are required. Similar considerations can be made for the dark green line shown in Fig. 11a, which represents the UFS trend. The UFS values reached by the specimens vary within a wider range than the one observed for the UTS trend, which is between about 51–87 MPa. The maximum UTS values are observed for the specimens obtained with 11, 13 and 15 printing conditions. The environmental impacts associated with the printing condition number 13 result as the lowest with respect to the other two (11, 15); thus, it could represent the best alternative when high flexural performances are required.

For what concerns Fig. 11b, the blue and dark green lines represent the E_t and E_f trends, respectively. The E_t values range between 1.7–2.7 GPa, with the highest values reached by specimens printed in conditions 2, 11 and 15. Since the lowest environmental impacts are those related to condition 2, it would represent the best trade-off when high tensile stiffness is required for a specific application. The E_f values vary within a range between 2.3–3.5 GPa and the highest values can be observed in correspondence of printing conditions number 7 and 11. The best trade-off condition could be the number 7 due to the low environmental impacts with respect to the 11 one.

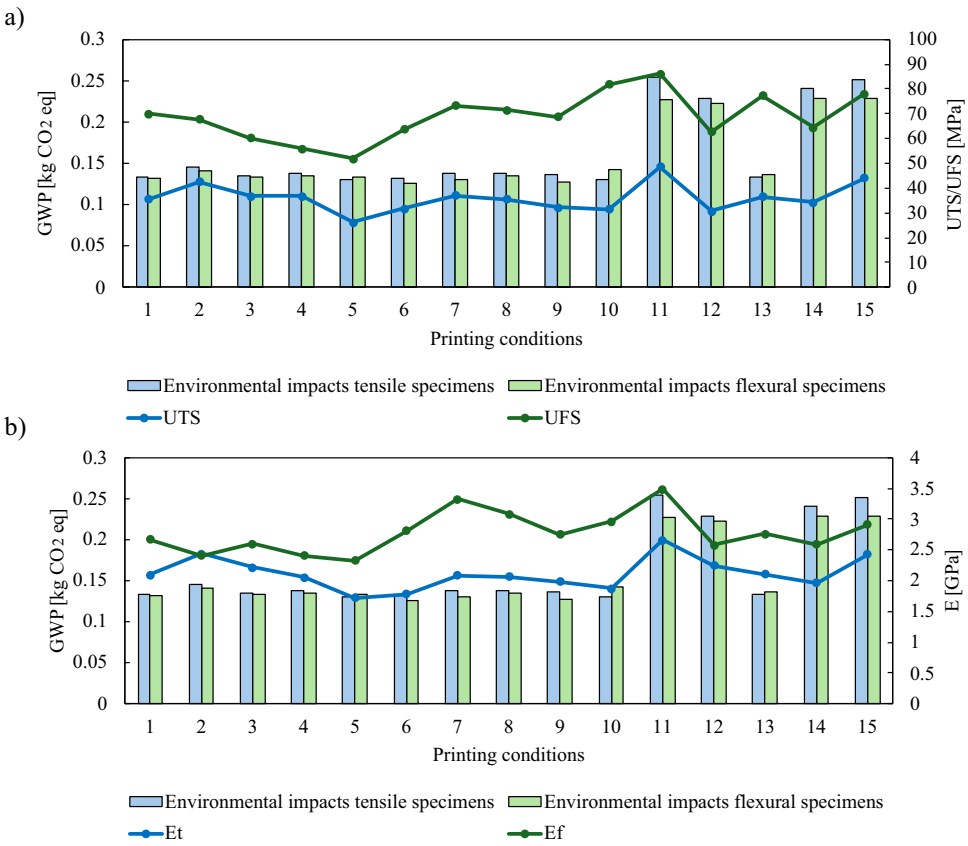

Fig. 11 Correlation between environmental impacts of both scenarios and all printing conditions and mechanical properties: UTS, UFS (**a**) and E_t, E_f (**b**)

These aspects are better investigated below by means of k_{UTS}, k_{UFS}, k_{Ef} and k_{Et} coefficients, defined in Sect. 2.4.3. These coefficients allow to numerically identify the printing condition which represents the most suitable solution according to the applications and involve low environmental impacts.

Figure 12 shows the trends of k coefficients as printing conditions vary; in particular, Fig. 12a represents k_{UTS} and k_{UFS} coefficients trends, while Fig. 12b highlights k_{Ef} and k_{Et} coefficients trends. Moreover, in both Fig. 12a and Fig. 12b a trend of medium values of coefficient k trend is reported, named k_m and k_{Em} respectively. The medium k values were evaluated to identify the best trade-off between the environmental impacts and the ultimate strength both under tensile and flexural loads (Fig. 12a) and between the environmental impacts and both tensile and flexural stiffness (Fig. 12b), with a unique value.

Figure 12a shows that printing condition number 2 results as the most suitable alternative to maintain low environmental impacts when a high tensile strength is required; while the number 10 represents the best alternative to obtain a low ecological footprint when high flexural strength is needed for a specific application. The k_M coefficient identifies the printing condition number 13 as the one which guarantees both good tensile and flexural strengths, by keeping low environmental impacts.

Figure 12b shows that printing condition number 2 results as the most suitable alternative to maintain low environmental impacts when a high tensile stiffness is required. When a high flexural stiffness is needed for a specific application, printing condition number 7 represents the best alternative to obtain a low ecological footprint. The same printing condition is identified by k_{Em} coefficient as the one which guarantees both good tensile and flexural stiffnesses, by keeping low environmental impacts.

Unlike previous investigations, which separately addressed either the mechanical behaviour or the environmental performance of MSLA printed components, the present work integrates experimental mechanical characterization, nonlinear predictive modelling and Life Cycle Assessment within a unified decision-making framework. This approach enables the identification of printing conditions that simultaneously maximize mechanical performance while minimizing environmental impacts, providing practical guidelines for sustainable MSLA manufacturing.

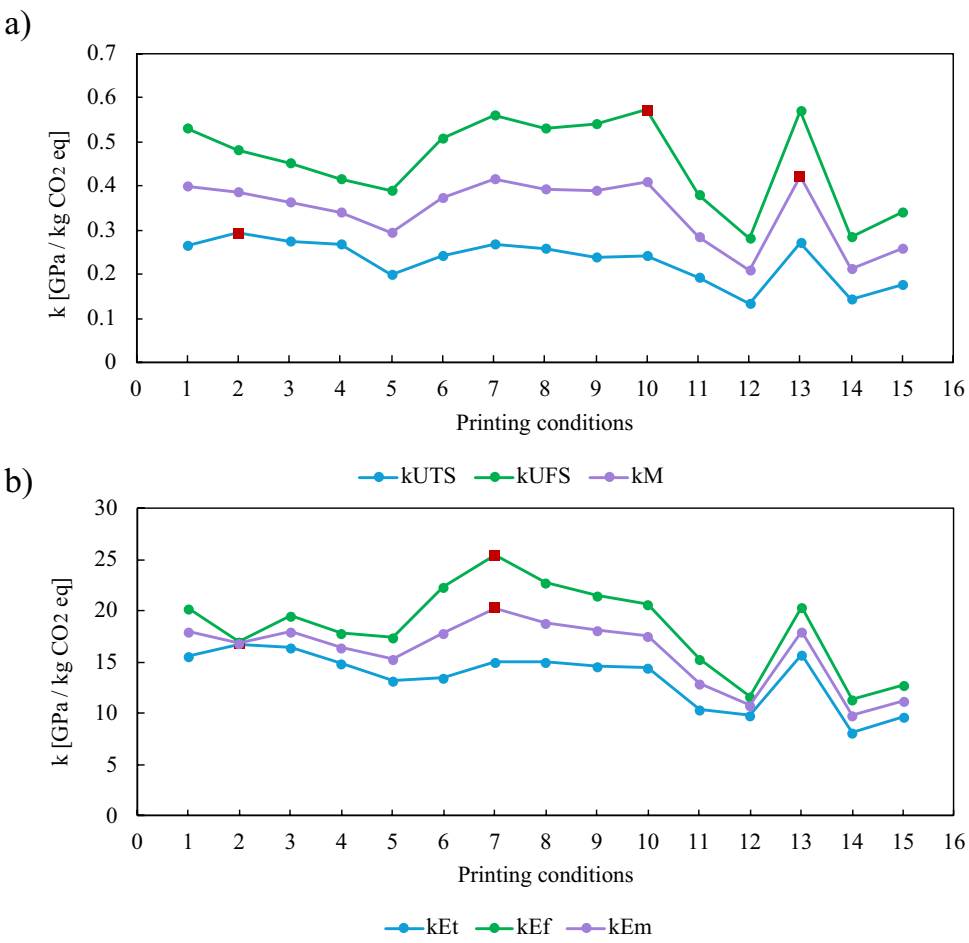

Fig. 12 k_{UTS}, k_{UFS}, k_{Ef} and k_{Et} coefficients trends as printing conditions vary

4 Conclusions

This study systematically investigated the influence of exposure time, layer thickness, and light intensity on the mechanical properties and energy consumption of parts fabricated using the Masked Stereolithography (MSLA) technique. Through tensile and flexural testing, combined with non-linear multiple regression analysis, several significant trends were identified, providing valuable insights for the optimization of printing parameters aimed at improving both mechanical performance and energy efficiency. In addition, the LCA analysis was conducted to define the 3D printing condition which balances high mechanical performances with reduced environmental impacts. Based on both the GWP impact category and the performance related to k coefficients, the following conclusions can be drawn:

- The results demonstrated that both tensile and flexural strengths are significantly affected by the chosen printing parameters. Longer exposure times (e.g., 12 s) and higher light intensities (e.g., 100%) generally enhanced mechanical performance, promoting greater polymer cross-linking and improved layer adhesion. However, diminishing returns were observed beyond specific thresholds, as confirmed by the negative quadratic terms in the regression models. Notably, the layer thickness exhibited a non-linear effect on mechanical properties, with optimal performance observed at intermediate thicknesses (0.045–0.055 mm). Thinner layers improved strength and modulus due to more homogeneous curing, while thicker layers often suffered from incomplete interlayer bonding.
- Energy consumption trends revealed a trade-off between mechanical performance and process efficiency. While thinner layers and longer exposure times enhanced mechanical properties, they also increased energy consumption due to longer print durations and higher cumulative light exposure. The regression models highlighted layer thickness as the most influential factor for energy consumption, with coarser layers significantly reducing power usage per specimen. Light intensity, though beneficial for mechanical strength, had a relatively modest impact on energy demands.
- All models demonstrated excellent predictive capabilities, with R^2 values above 96% and MAPE below 8%, affirming the robustness and accuracy of the regression equations. The residual plots further confirmed the absence of significant bias or heteroscedasticity in most cases. The small deviations observed in a few models (notably UFS and EC_f) are limited and do not compromise the overall reliability of the results. These findings validate the use of the developed models for predicting mechanical properties and energy efficiency in additive manufacturing processes.
- The environmental impacts are similar between the two analyzed scenarios for all considered printing conditions. In particular, printing conditions characterized by lower layer thickness value (e.g. conditions 11, 12, 14 and 15) showed the highest values of environmental impacts due to the increase of the material used and the energy consumption related to extended printing times.
- For all analyzed conditions and scenarios, the material phase resulted as the most impactful one, accounting for 78–92% and 77–93% of total emissions in Scenarios 1 and 2, respectively.
- The evaluation of trade-offs between the mechanical performances and the environmental impacts showed that printing condition 2 represents the best solution to obtain good UTS values with a low ecological footprint; while, to obtain high UFS values, the most suitable alternative is printing condition 13. To achieve high tensile stiffness values, printing condition 2 emerges as the most balanced choice, while for high flexural stiffness values printing condition number 7 demonstrates the best trade-off.
- The medium k coefficients highlight condition 13 as the most effective all-around solution when both tensile and flexural strength are considered; while for stiffness-related applications, condition 7 proves to be the best compromise.

The non-linear regression models developed in this work accurately captured the complex relationships between process parameters and performance metrics. These models can serve as predictive tools to identify optimal parameter sets that balance mechanical performance with energy efficiency.

Thuse, printing condition 2 consistently stands out for tensile-based applications, while conditions 7 and 13 are suitable for stiffness and overall strength, respectively. These findings provide a robust decision-making framework to select optimal printing parameters in sustainability-conscious manufacturing contexts.

Although the proposed methodology proved effective in identifying the optimal balance between mechanical performance and environmental sustainability, some limitations of the present study should be acknowledged. The investigation was conducted using a single commercial photocurable resin and one MSLA printing system; therefore, the developed regression models should be considered valid within the investigated material–process combination. Moreover, only three process parameters (exposure time, layer thickness and LED intensity) were varied, while other factors,

such as build orientation, post-curing conditions, ambient temperature and resin ageing, may also influence the final mechanical performance. From an environmental perspective, the assessment was limited to a cradle-to-gate system boundary and the Global Warming Potential impact category. Future work will focus on extending the proposed methodology to different MSLA platforms, engineering-grade photopolymers and functional materials, additional processing parameters, and on validating the predictive models through independent experimental datasets. Furthermore, the environmental assessment will be expanded to a cradle-to-grave perspective by considering additional impact categories, in order to provide a more comprehensive sustainability evaluation and assess the applicability of the proposed integrated optimization framework across a broader range of MSLA applications.

Appendix A

The coefficients for the mathematical model to evaluate the Elasticity Tensile modulus.

Coefficient	Value
A_0	0.93
A_1	14.6
A_2	-4.77
A_3	-0.092
A_4	-118
A_5	3.66
A_6	0.00315

The coefficients for the mathematical model to evaluate the Ultimate Tensile Strength (UTS).

Coefficient	Value
B_0	4.22
B_1	-144
B_2	46.9
B_3	-0.297
B_4	759
B_5	-21.9
B_6	0.0088

The coefficients for the mathematical model to evaluate the Elasticity Flexural modulus.

Coefficient	Value
C_0	0.691
C_1	-7.3
C_2	3.54
C_3	-0.087
C_4	57
C_5	-2.46
C_6	0.00352

The coefficients for the mathematical model to evaluate the Ultimate Flexural Strength (UFS).

Coefficient	Value
D_0	22.2
D_1	-297
D_2	41
D_3	-2.66
D_4	2484
D_5	-25.5
D_6	0.105

The coefficients for the mathematical model to evaluate the energy consumption of five tensile specimens.

Coefficient	Value
E_0	0.0495
E_1	-2.88
E_2	0.007
E_3	-0.00644
E_4	18.8
E_5	0.013
E_6	0.000272

The coefficients for the mathematical model to evaluate the energy consumption of five Flexural specimens.

Coefficient	Value
F_0	0.0552
F_1	-3.201
F_2	0.001
F_3	0.00749
F_4	21.98
F_5	0.0187
F_6	0.000322

Authors' contributions Chiara Mignanelli: Writing, Formal analysis, Investigation. Michela Simoncini: Writing- Reviewing and Editing, Investigation, Visualization. Tommaso Verdini: Data curation, Writing, Methodology, Investigation.

Funding Open access funding provided by Università Politecnica delle Marche within the CRUI-CARE Agreement.

Data availability The data that support the findings of this study are available from the corresponding author upon reasonable request.

Declarations

Competing interest The authors declare that they have no known competing financial interests or personal relationships that could have appeared to influence the work reported in this paper.

Open Access This article is licensed under a Creative Commons Attribution 4.0 International License, which permits use, sharing, adaptation, distribution and reproduction in any medium or format, as long as you give appropriate credit to the original author(s) and the source, provide a link to the Creative Commons licence, and indicate if changes were made. The images or other third party material in this

article are included in the article's Creative Commons licence, unless indicated otherwise in a credit line to the material. If material is not included in the article's Creative Commons licence and your intended use is not permitted by statutory regulation or exceeds the permitted use, you will need to obtain permission directly from the copyright holder. To view a copy of this licence, visit http://creativecommons.org/licenses/by/4.0/.

References

1. Bianchi I, Forcellese A, Mancia T, Simoncini M (2023) Tensile properties and sustainability assessment of vat photopolymerization 3D printed components with recovered plastic filler. Int J Adv Manuf Technol 129:2171–2182. https://doi.org/10.1007/S00170-023-12412-Y/FIGURES/10
2. Pusateri V, Hauschild MZ, Kara S et al (2024) Quantitative sustainability assessment of metal additive manufacturing: a systematic review. CIRP J Manuf Sci Technol 49:95–110. https://doi.org/10.1016/J.CIRPJ.2023.12.005
3. Galeta T, Raos P, Stojšić J, Pakši I (2016) Influence of structure on mechanical properties of 3D printed objects. Procedia Eng 149:100–104. https://doi.org/10.1016/J.PROENG.2016.06.644
4. Bonada J, Muguruza A, Fernández-Francos X, Ramis X (2017) Influence of exposure time on mechanical properties and photocuring conversion ratios for photosensitive materials used in additive manufacturing. Procedia Manuf 13:762–769. https://doi.org/10.1016/J.PROMFG.2017.09.182
5. Engineering Journal Al A-K, Raed Mhmood T, Kais Al-Karkhi N (2023) A Review of the Stereo lithography 3D Printing Process and the Effect of Parameters on Quality. Al-Khwarizmi Eng J 19:82–94. https://doi.org/10.22153/KEJ.2023.04.003
6. Orzeł B, Stecuła K (2022) Comparison of 3D printout quality from FDM and MSLA technology in unit production. Symmetry (Basel) 14:910. https://doi.org/10.3390/SYM14050910
7. Msallem B, Sharma N, Cao S et al (2020) Evaluation of the Dimensional Accuracy of 3D-Printed Anatomical Mandibular Models Using FFF, SLA, SLS, MJ, and BJ Printing Technology. J Clin Med 9:817. https://doi.org/10.3390/JCM9030817
8. Huang J, Qin Q, Wang J (2020) A Review of Stereolithography: Processes and Systems. Processes 8:1138. https://doi.org/10.3390/PR8091138
9. Ge Q, Li Z, Wang Z et al (2020) Projection micro stereolithography based 3D printing and its applications. Int J Extreme Manuf 2:022004. https://doi.org/10.1088/2631-7990/AB8D9A
10. Milovanović A, Montanari M, Golubović Z et al (2024) Compressive and flexural mechanical responses of components obtained through mSLA vat photopolymerization technology. Theor Appl Fract Mech 131:104406. https://doi.org/10.1016/J.TAFMEC.2024.104406
11. Borra ND, Neigapula VSN (2023) Parametric optimization for dimensional correctness of 3D printed part using masked stereolithography: Taguchi method. Rapid Prototyp J 29:166–184. https://doi.org/10.1108/RPJ-03-2022-0080/FULL/PDF
12. Temiz A (2023) The Effects of Process Parameters on Tensile Characteristics and Printing Time for Masked Stereolithography Components, Analyzed Using the Response Surface Method. J Mater Eng Perform 33:9356–9365. https://doi.org/10.1007/S11665-023-08617-7/TABLES/6
13. Štaffová M, Ondreáš F, Svatík J et al (2022) 3D printing and post-curing optimization of photopolymerized structures: basic concepts and effective tools for improved thermomechanical properties. Polym Test 108:107499. https://doi.org/10.1016/J.POLYMERTESTING.2022.107499
14. Valizadeh I, Tayyarian T, Weeger O (2023) Influence of process parameters on geometric and elasto-visco-plastic material properties in vat photopolymerization. Addit Manuf 72:103641. https://doi.org/10.1016/J.ADDMA.2023.103641
15. Temiz A (2024) The tensile properties of functionally graded materials in MSLA 3D printing as a function of exposure time. J Mater Mechat A 5:49–59. https://doi.org/10.55546/JMM.1413577
16. Kim D, Shim JS, Lee D et al (2020) Effects of post-curing time on the mechanical and color properties of three-dimensional printed crown and bridge materials. Polymers (Basel) 12:2762. https://doi.org/10.3390/POLYM12112762
17. Martín-Montal J, Pernas-Sánchez J, Varas D (2021) Experimental characterization framework for SLA additive manufacturing materials. Polymers (Basel) 13:1147. https://doi.org/10.3390/POLYM13071147
18. Raul Fernandez-Vidal S, Vieira Da Cunha T, Neural A, Ali Abdulkader Kadauw A (2025) Neural Network Optimization of Mechanical Properties of ABS-like Photopolymer Utilizing Stereolithography (SLA) 3D Printing. J Manuf Mater Process 9:116. https://doi.org/10.3390/JMMP9040116
19. Chockalingam K, Jawahar N, Ramanathan KN, Banerjee PS (2006) Optimization of stereolithography process parameters for part strength using design of experiments. Int J Adv Manuf Technol 29:79–88. https://doi.org/10.1007/S00170-004-2307-0/METRICS
20. Quintana R, Choi JW, Puebla K, Wicker R (2010) Effects of build orientation on tensile strength for stereolithography- manufactured ASTM D-638 type i specimens. Int J Adv Manuf Technol 46:201–215. https://doi.org/10.1007/S00170-009-2066-Z/METRICS
21. Mhmood TR, AL-Karkhi NK (2023) Multiobjective optimization of stereolithography for dental bridge based on a simple shape model using Taguchi and response surface methods. Appl Sci (Basel) 13:10911. https://doi.org/10.3390/APP131910911
22. Weheba G, Sanchez-Marsa A (2006) Using response surface methodology to optimize the stereolithography process. Rapid Prototyp J 12:72–77. https://doi.org/10.1108/13552540610652401/FULL/XML
23. Singh S, Jain A, Chaudhary P et al (2023) Optimization of dimensional accuracy and surface roughness in m-SLA using response surface methodology. Rapid Prototyp J 29:1324–1339. https://doi.org/10.1108/RPJ-05-2022-0158
24. Cotabarren I, Palla CA, McCue CT, Hart AJ (2019) An assessment of the dimensional accuracy and geometry-resolution limit of desktop stereolithography using response surface methodology. Rapid Prototyp J 25:1169–1186. https://doi.org/10.1108/RPJ-03-2019-0060/FULL/PDF
25. Mele M, Campana G, D'Avino G (2020) Life cycle impact assessment of desktop stereolithography. J Clean Prod 244:118743. https://doi.org/10.1016/J.JCLEPRO.2019.118743
26. Al Rashid A, Khan SA, Koç M (2024) Life cycle assessment on fabrication and characterization techniques for additively manufactured polymers and polymer composites. Cleaner Environ Syst 12:100159. https://doi.org/10.1016/J.CESYS.2023.100159
27. Khan SA, Jassim M, Ilcan H et al (2023) 3D printing of circular materials: comparative environmental analysis of materials and construction techniques. Case Stud Constr Mater 18:e02059. https://doi.org/10.1016/J.CSCM.2023.E02059
28. Yadav A, Garg RK, Sachdeva A, Qureshi MRNM (2025) Comparing environmental sustainability of additive manufacturing and investment casting: life cycle assessment of Aluminium LM04 (Al-Si5-Cu3). Mater Sci Eng A 923:147765. https://doi.org/10.1016/J.MSEA.2024.147765

Publisher's note Springer Nature remains neutral with regard to jurisdictional claims in published maps and institutional affiliations.